

OCT 28 1957

UNCLASSIFIED
~~CONFIDENTIAL~~

Copy

4

RM A57H19a

c.1

NACA RM A57H19a

NACA

RESEARCH MEMORANDUM

A TRANSONIC INVESTIGATION OF THE EFFECTS OF SEMISUBMERGED-
STORE CAVITIES AND OF SLOTS ON THE ZERO-LIFT DRAG OF
A BODY OF REVOLUTION

By George H. Holdaway, Minor R. Wallace, Jr.,
and Elaine W. Hatfield

Ames Aeronautical Laboratory
Moffett Field, Calif.

LIBRARY COPY

OCT 29 1957

CLASSIFICATION CHANGED

UNCLASSIFIED

LANGLEY AERONAUTICAL LABORATORY
LIBRARY, NACA
LANGLEY FIELD, VIRGINIA

To _____

By authority of *NASA TPA 9 E. Hestine* Date *9-1-57*
7B 11-25-57
CLASSIFIED DOCUMENT

This material contains information affecting the National Defense of the United States within the meaning of the espionage laws, Title 18, U.S.C., Sec. 793 and 794, the transmission or revelation of which in any manner to an unauthorized person is prohibited by law.

NATIONAL ADVISORY COMMITTEE FOR AERONAUTICS

WASHINGTON
October 28, 1957

~~CONFIDENTIAL~~
UNCLASSIFIED



NATIONAL ADVISORY COMMITTEE FOR AERONAUTICS

RESEARCH MEMORANDUM

A TRANSONIC INVESTIGATION OF THE EFFECTS OF SEMISUBMERGED-
STORE CAVITIES AND OF SLOTS ON THE ZERO-LIFT DRAG OF
A BODY OF REVOLUTION

By George H. Holdaway, Minor R. Wallace, Jr.,
and Elaine W. Hatfield

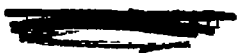
SUMMARY

A systematic study of various sized cavities and slots in bodies of revolution was conducted over a Mach number range of 0.80 to 1.20 and at a Reynolds number of about 36,000,000 based on the body length. The resultant body cross-sectional area distributions were in each case the same as that for a Sears-Haack body. The zero-lift drag characteristics due to friction, separated flow, and compression waves were analyzed.

The results of this investigation indicated that cavities with fineness ratios of 8 or greater can be used to control the body area distribution without introducing unpredicted changes or penalties in wave drag; however, cavities in general tend to produce separated flow with an accompanying increase in drag at all Mach numbers. Symmetrical slot arrangements with gradual changes in depth can be used to control the area distribution of bodies without penalties in wave drag and very little drag resulting from separated flow, but generally with a predictable penalty in friction drag. For the reference bodies of revolution, linearized theory generally overestimated the wave drag at transonic speeds.

INTRODUCTION

The problem of carrying external stores on airplanes with the least drag penalty is one which continually challenges the designer. One method of coping with the problem is to utilize semisubmerged stores in fuselage cavities or rockets in fuselage slots. With the stores in place, the airplane can be designed to have a smooth area distribution with low wave drag at a specified Mach number in accordance with the concepts of reference 1, 2, or 3. With the stores removed the localized indentations or cavities might be utilized to obtain low wave drag at a second design



UNCLASSIFIED

Mach number. However some of these cavities may have drag penalties, resulting from separated flow or increased surface area, which could counter any improvements in wave drag. Such viscous-drag penalties have been evident in the experimental results of prior investigations of cavities reported in references 4, 5, and 6.

The investigation reported herein was planned to illustrate the magnitude of the different drag components associated with various localized indentations and to indicate the type and size of localized indentations for which the wave-drag theory is applicable and for which there are no large penalties in viscous drag. The bodies in each case were designed to have the same theoretical wave drag at a Mach number of 1 (i.e., the same basic area distribution) but different indentations, thus any experimental variation in wave drag from that of the basic body would be an indication of a violation or limitation of the concepts involved.

A systematic study was made in the Ames 14-foot transonic wind tunnel of the two general classes of localized indentations mentioned previously: single-store cavities and slots. One cavity was used per body, and all the cavities had the same length but had variations in fineness ratio of 4 to 9. The slots had the same length as the cavities, and the number per body varied from 1 to 32.

Force data, schlieren photographs, and base pressures were obtained at zero lift over a Mach number range of 0.80 to 1.20 at a Reynolds number of approximately 36,000,000 based on the body length.

SYMBOLS

a	radius of cavity
b	distance from body center line to store center line
C_{D_0}	zero-lift drag coefficient
ΔC_{D_0}	experimental drag-rise coefficient above subsonic level at M = 0.80
c	slot side depth
d	slot center depth relative to body radius
f	fineness ratio
l	fuselage length
M	free-stream Mach number

N number of terms or harmonics used in the Fourier sine series
r local radius of body
 r_0 maximum radius of body 1
S body cross-sectional area normal to x axis
w slot width
x,y,z Cartesian coordinates as conventional body axes

MODELS AND TESTS

The basic body (body 1) used for this investigation was a Sears-Haack type (minimum-wave-drag body for prescribed volume and length) with a closed-body fineness ratio of 12.5. All models tested, except body 8, had the same cross-sectional area distribution (equal theoretical wave drag for $M = 1.00$) as that for the basic body. Body 8, which was another reference body for the tests, had an area distribution essentially equal to that of body 1 plus the addition of a fineness-ratio-6 semisubmerged store. The area distributions for bodies 1 and 8 are presented in figure 1. The equation for body 1 and representative sketches of the bodies with either a cavity or slots are presented in figure 2. The volume removed by the cavity in each case was added around the remainder of the body so as to maintain the same cross-sectional area distribution as that for body 1. For the slotted bodies the external contour of body 8 was maintained and the volume removed by the slots was such that the same area distribution as that of body 1 was again maintained. The bodies were cut off at the base to permit mounting the models on a sting, which resulted in a ratio of base diameter to sting diameter of 1.211. All of the cavities and slots were 20 inches in length or about one quarter of the actual body length. A brief description of the 14 primary bodies is given in the following table.

<u>Body</u>	<u>Description</u>
1	Basic body - Sears-Haack, $f = 12.5$, $r_0 = 3.5$ inches
2	$f = 4$ store cavity, volume = body 1
3	$f = 5$ store cavity, volume = body 1
4	$f = 6$ store cavity, volume = body 1
5	$f = 7$ store cavity, volume = body 1
6	$f = 8$ store cavity, volume = body 1
7	$f = 9$ store cavity, volume = body 1
8	Body 4 without cavity, volume \neq body 1
9	Body 8 with 32 slots, 0.1 in. wide volume = body 1
10	Body 8 with 16 slots, 0.2 in. wide volume = body 1
11	Body 8 with 8 slots, 0.4 in. wide volume = body 1
12	Body 8 with 4 slots, 0.8 in. wide volume = body 1
13	Body 8 with 2 slots, 1.6 in. wide volume = body 1
14	Body 8 with 1 slot, 1.6 in. wide volume = body 1

The single slot of body 14 had a maximum depth which was about twice as great as the corresponding depths of the slots for the other slotted bodies. The lower halves of the central segments of bodies 2 through 7 (with cavities) are shown in figure 3, and the lower halves of the central segments of bodies 9 through 14 (with slots) are shown in figure 4. The effect of asymmetrical slot positioning on the drag characteristics was investigated by modifying body 13. The modification placed the two slots in an asymmetrical arrangement with the centers of the slots displaced 49° , as shown in figure 5. For body 13 the slots were displaced 180° .

The effect of fairing the edges of a cavity on the aerodynamic characteristics was investigated with body 2 which had the deepest cavity. Three modifications to the cavity edges of body 2 were made from the $1/16$ -inch-edge radius common to all the cavities. Modification 1 was a 10° bevel at the front and at the rear of the cavity, measured in the streamwise direction, and 0.3 of an inch down from the apex of the cavity. Modification 2 was a further smoothing of just the rearward edges of the cavity as shown in figure 6. Modification 3, also shown in figure 6, was similar to modification 2 except both the forward and rearward edges were smoothed. These modifications, the dimensions of which are tabulated in table I(c), had an insignificant effect on the total area distribution.

The bodies were tested in the Ames 14-foot transonic wind tunnel which is of the closed-return type with perforated walls in the test section. A sketch of the high-speed regions of this test facility is presented in figure 7. The flexible walls ahead of the test section are controlled to produce the convergent-divergent nozzle form required to generate Mach numbers up to 1.20. This tunnel is similar to the smaller, Ames 2- by 2-foot transonic wind tunnel which is described in reference 7. One exception, however, is that the 14-foot tunnel is not of the variable-density type, but operates at atmospheric pressure. Models are mounted on a sting as shown in figure 8, and the forces are measured as electrical

outputs from a strain-gage balance located within the model. Figure 8 also shows the fixed-transition grit (size 200) distributed over 1 inch of the nose of body 1. Transition of the boundary layer was similarly fixed for all the tests.

Force data, schlieren photographs, and base pressures were obtained at zero lift over a Mach number range of 0.80 to 1.20 at a Reynolds number of about 36,000,000 based on the body length of 79.62 inches. The drag coefficients are based on the maximum cross-sectional area of body 1, and were corrected for base effects by adjusting the base pressures to free-stream static pressure. The tunnel blockage of body 8 was 0.16 percent and all the other bodies had a tunnel blockage of 0.14 percent.

Two parts of the total drag were estimated by theoretical computations. Friction drag was estimated from the charts of reference 8 and the wave drag was estimated from the harmonic analysis method of reference 9 using 25 harmonics. No method was known for predicting drag due to separated flow.

RESULTS AND DISCUSSION

The zero-lift drag coefficients for the unindented bodies 1 and 8 will be presented and discussed first, because body 1 represents the minimum-drag goal of all the indented bodies and body 8 represents the upper wave-drag limit expected for the slotted bodies neglecting changes in friction drag. The next part of this section of the report will present and discuss the drag data for the bodies with single-store cavities including the effect of smoothing the edges of the lowest fineness-ratio cavity, body 2. The last part will present and discuss the drag data for the bodies with slots including the effects of an asymmetrical location of the slots.

Unindented Bodies

The zero-lift drag coefficients for bodies 1 and 8 are presented in figure 9. These two bodies had similar computed friction-drag coefficients and experimental base-drag coefficients (within the accuracy of the data). These base-drag coefficients are also similar to the values obtained with all the bodies. At subsonic speeds without separated flow, the pressure drag is theoretically zero, and thus the total drag should be just friction drag. Note that adding the negative base-drag correction to the data points results in subsonic drag coefficients which are closely estimated by the computed friction-drag coefficients. These results indicate that separated flow did not occur for the two reference unindented bodies. The lower half of figure 9 compares the experimental drag-rise coefficients

above the subsonic coefficients at $M = 0.80$ with computed wave-drag coefficients (corrected for friction-drag-coefficient variation with Mach number). There is a wave-drag-coefficient difference between the two bodies which is almost constant with Mach number. It is of interest to note that at transonic speeds linearized theory generally overestimates the wave drag of the unindented bodies of revolution. This same effect was found in reference 10, but occurred primarily for bodies with lower fineness ratios.

Bodies With Cavities

The experimental drag coefficients are plotted in figure 10 as a function of Mach number for all the bodies with cavities. The computed friction-drag coefficients for all these bodies were very nearly the same. As the cavity fineness ratio is progressively decreased, there is an obvious large increase in the drag coefficients at $M = 0.80$ which must be due to separated flow. The variation of the drag coefficients with cavity fineness ratio can be further demonstrated by selecting two representative Mach numbers ($M = 1.00$ and 1.20) and plotting the data as a function of fineness ratio as shown in figure 11. The drag data for these bodies with cavities are compared with body 1, because each body had the same cross-sectional area distribution as body 1 and hence the same theoretical wave drag at $M = 1.00$. The general trends of the drag variation with fineness ratio are the same at $M = 1.20$ as at the design Mach number ($M = 1.00$). Only for the highest fineness-ratio cavity was the value of body 1 drag approached. Cavities of fineness ratios of 6 or less not only had greater separation drag but also a marked increase in the wave drag above that of body 1 as shown in figure 12. These lower fineness-ratio cavities apparently violate the slenderness limitation of the theory. There is also additional evidence that the shock waves produced by the bump on the bodies were not eliminated by the cavity and thus the wave drag would be greater than that for the basic body. There were no shock waves evident at supersonic speeds in the schlieren photographs of the central region of the basic body (body 1). However, photographs of body 2 (fig. 13(a)) with the deepest cavity revealed the presence of shocks on the upper surface of the body near the edges of the bump. At supersonic speeds shocks on the cavity side of the body were nonexistent or very weak.

The separated flow resulting from the cavities was observed by positioning the knife edge of the schlieren system to accentuate the boundary-layer flow as shown for body 2 with modification 2 in figure 13(b). The presence of separated flow or a mixing region is clearly indicated in this picture and, since the boundary-layer wake effectively changes the body shape, it is clear there would be an increase in wave drag as well as a separation drag. The reduction in the size of the wake with increased fineness ratio is illustrated in the schlieren photographs of figure 14.

The large amounts of drag attributed to separated flow for the lower fineness-ratio cavities are partially due to the abrupt change in contour at the edges of the cavities. Body 2 had the deepest cavity and the largest amount of separation drag, therefore this body was selected to evaluate the reduction in separation drag that could be obtained by fairing the edges of the cavity. The results of tests to determine the effect of the three modifications to body 2 on the drag coefficients are presented in figure 15. Note that the drag coefficients were progressively reduced by smoothing the forward and rearward edges of the cavity. The experimental rise in drag coefficient with Mach number for all three modifications was essentially the same. As mentioned in the description of the models, the modifications had little effect on the area distribution of body 2, thus the various modifications would not alter the computed wave-drag coefficients. In keeping with the prior discussion in this paragraph, note in figure 15 that the rise in drag coefficients with Mach number for body 2 is greater than the computed values. It should be pointed out that for Mach numbers above 1.00 the computed wave-drag coefficients are greater for body 2 than for body 1.

Bodies With Slots

The experimental drag-coefficient results are plotted in figure 16 as a function of Mach number for the bodies with slots. For these bodies the computed friction-drag coefficients are a direct function of the number of slots as well as the Mach number. The results for $M = 1.00$ and 1.20 are plotted in figure 17 as a function of the number of slots to illustrate better the variation in the drag coefficients with the number of slots. Note that all the slotted bodies have the same area distribution as body 1 and that the drag for body 8 is the zero-slot reference value shown in figure 17. The drag of the slotted bodies was consistently greater than that for body 1 and generally greater than that for body 8. The drag increase of the body with two slots, relative to body 1, is attributed to slight increases in friction drag and in drag due to separated flow along the sharp edges and corners of the slots. The increase in drag with the increase in the number of slots up to 16 was directly comparable to the predicted increase in friction drag. For the body with 32 slots, the slot width at the mid-length position was only about twice the boundary-layer displacement thickness. Thus, this body with 32 slots evidently had less experimental friction drag than that computed, as a result of the reduction of velocity of the air in the slots.

The greater drag for the body with one slot when compared with the trend of the drag with the number of slots was attributed primarily to the greater depth (about twice) of this slot. This greater depth, or rate of change in depth with length, was thought to result in separated or mixed flow comparable to that of the models with the low-fineness-ratio cavities. This supposition was partially confirmed by the additional test

of body 13 with two slots located asymmetrically in one quadrant of the cross section. The drag coefficients from this test are plotted in figure 18 with data for the bodies with one slot (body 14) and with two symmetrically located slots (body 13). At subsonic Mach numbers the increased drag due to flow separation, of the body with one deep slot, is not present for the comparably asymmetrical two-slot body. At supersonic Mach numbers changing the two-slot body from a symmetrical to an asymmetrical arrangement did result in a slight penalty in drag-rise coefficient.

All the symmetrically slotted bodies were effective in removing the wave-drag increment caused by the bump of body 8. As shown in figure 19 all the slotted bodies, except for the body with one slot, had drag-rise coefficients equal to or less than that for body 1.

CONCLUSIONS

The results of this transonic investigation of bodies with cavities and slots indicate the following:

1. Cavities with fineness ratios of 8 or greater can be used to control the body area distribution without introducing unpredicted changes or penalties in wave drag; however, cavities, in general, tend to produce a drag increase resulting from separated or mixed flow.
2. Symmetrical slot arrangements with gradual changes in depth can be used to control the area distribution of bodies without penalties resulting from increased wave drag and very little drag resulting from separated flow, but with a penalty in friction drag which appears to be predictable.
3. Slots with a large rate of change in depth with length and cavities with low fineness ratio tend to increase the separation drag.
4. For the reference bodies of revolution, linearized theory generally overestimated the wave drag at transonic speeds.

Ames Aeronautical Laboratory
National Advisory Committee for Aeronautics
Moffett Field, Calif., Aug. 19, 1957

REFERENCES

1. Whitcomb, Richard T.: A Study of the Zero-Lift Drag-Rise Characteristics of Wing-Body Combinations Near the Speed of Sound. NACA RM L52H08, 1952.
2. Jones, Robert T.: Theory of Wing-Body Drag at Supersonic Speeds. NACA Rep. 1284, 1956. (Supersedes NACA RM A53H18a.)
3. Lomax, Harvard: The Wave Drag of Arbitrary Configurations in Linearized Flow as Determined by Areas and Forces in Oblique Planes. NACA RM A55A18, 1955.
4. Hoffman, Sherwood, and Wolff, Austin L.: Effect on Drag of Longitudinal Positioning of Half-Submerged and Pylon-Mounted Douglas Aircraft Stores on a Fuselage With and Without Cavities Between Mach Numbers of 0.9 and 1.8. NACA RM L54E26, 1954.
5. Mason, Homer P., and Henning, Allen B.: Effects of Some External-Store Mounting Arrangements and Store Shapes on the Buffet and Drag Characteristics of Wingless Rocket-Powered Models at Mach Numbers from 0.7 to 1.4. NACA RM L54I20a, 1954.
6. Hoffman, Sherwood: Zero-Lift Drag of a Large Fuselage Cavity and a Partially Submerged Store on a 52.5° Sweptback-Wing-Body Configuration as Determined from Free-Flight Tests at Mach Numbers of 0.7 to 1.53. NACA RM L56L21, 1957.
7. Spiegel, Joseph M., and Lawrence, Leslie F.: A Description of the Ames 2- by 2-Foot Transonic Wind Tunnel and Preliminary Evaluation of Wall Interference. NACA RM A55I21, 1956.
8. Lee, Dorothy B., and Faget, Maxime A.: Charts Adapted from Van Driest's Turbulent Flat-Plate Theory for Determining Values of Turbulent Aerodynamic Friction and Heat-transfer Coefficients. NACA TN 3811, 1956.
9. Holdaway, George H., and Mersman, William A.: Application of Tchebichef Form of Harmonic Analysis to the Calculation of Zero-Lift Wave Drag of Wing-Body-Tail Combinations. NACA RM A55J28, 1956.
10. Nelson, Robert L., and Walsh, Clement J.: Some Examples of the Applications of the Transonic and Supersonic Area Rules to the Prediction of Wave Drag. NACA RM L56D11, 1957.

TABLE I.- COORDINATES OF BODIES
(a) Bodies 2 through 7 with cavities

Body station x	Body 2 f=4		Body 3 f=5		Body 4 f=6		Body 5 f=7		Body 6 f=8		Body 7 f=9	
	r	a	r	a	r	a	r	a	r	a	r	a
0	Radii the same for all bodies.											
↓	See figure 2 for basic body shape and equation.											
33.75	3.361	0	3.370	0	3.369	0	3.368	0	3.368	0	3.368	0
33.94	3.371	.213	3.378	.171	3.376	.142	3.375	.122	3.375	.107	3.374	.095
34.13	3.382	.357	3.431	.286	3.420	.238	3.413	.204	3.409	.179	3.406	.159
35.00	3.451	.842	3.491	.674	3.468	.561	3.453	.481	3.446	.421	3.439	.374
35.88	3.532	1.211	3.550	.969	3.515	.807	3.494	.692	3.480	.606	3.471	.538
36.75	3.614	1.509	3.608	1.207	3.560	1.005	3.532	.862	3.513	.754	3.500	.670
37.63	3.694	1.758	3.639	1.407	3.629	1.172	3.609	1.005	3.603	.879	3.586	.781
39.38	3.835	2.133	3.709	1.706	3.695	1.421	3.667	1.219	3.629	1.066	3.603	.948
41.13	3.934	2.370	3.817	1.896	3.724	1.580	3.670	1.355	3.629	1.185	3.586	1.053
42.88	3.985	2.486	3.822	1.989	3.727	1.657	3.670	1.421	3.632	1.243	3.605	1.105
43.75	3.992	2.500	3.817	2.000	3.724	1.666	3.667	1.429	3.629	1.250	3.603	1.111
44.62	3.985	2.486	3.817	1.989	3.724	1.657	3.667	1.421	3.629	1.243	3.603	1.105
46.37	3.934	2.370	3.822	1.896	3.727	1.580	3.670	1.355	3.629	1.185	3.586	1.053
48.12	3.835	2.133	3.709	1.706	3.639	1.421	3.597	1.219	3.570	1.066	3.551	.948
49.87	3.694	1.758	3.608	1.407	3.560	1.172	3.532	1.005	3.513	.879	3.500	.781
50.75	3.614	1.509	3.550	1.207	3.515	1.005	3.494	.862	3.480	.754	3.471	.670
51.62	3.532	1.211	3.491	.969	3.468	.807	3.453	.692	3.446	.606	3.439	.538
52.50	3.451	.842	3.431	.674	3.420	.561	3.413	.481	3.409	.421	3.406	.374
53.37	3.382	.357	3.378	.286	3.376	.238	3.375	.204	3.375	.179	3.374	.159
53.56	3.371	.213	3.370	.171	3.369	.142	3.368	.122	3.368	.107	3.368	.095
53.75	3.361	0	3.370	0	3.369	0	3.368	0	3.368	0	3.368	0
79.62	1.514											
	Radii the same for all bodies											

Note: Columns a are cavity radii with centers 3.361 inches from body center line. All dimensions are in inches.

TABLE I.- COORDINATES OF BODIES - Continued
 (b) Bodies 8 through 14 with slots

Station x	Body 8	Body 9			Body 10			Body 11			Body 12			Body 13			Body 14			
	Body 4 without indentation	32 slots			16 slots			8 slots			4 slots			2 slots			1 slot			
	Radial	w	d	c	w	d	c	w	d	c	w	d	c	w	d	c	w	d	c	
0	Radii the same for all bodies. See figure 2 for basic body shape and equation.																			
33.75	3.361	0	0	0	0	0	0	0	0	0	0	0	0	0	0	0	0	0	0	
33.94	3.369	.100	.012	.012	.200	.012	.011	.400	.014	.008	.750	.021	0	.920	.032	0	1.150	.049	0	
34.13	3.376		.026	.026		.027	.026		.029	.023	.800	.035	.011	1.202	.054	0	1.500	.084	0	
35.00	3.420		.170	.170		.171	.170		.173	.167		.178	.135	1.600	.202	.107	1.600	.373	.278	
35.88	3.468		.358	.358		.358	.357		.360	.354		.366	.343		.390	.296		.748	.654	
36.75	3.515		.563	.563		.562	.561		.564	.558		.570	.547		.592	.500		1.154	1.062	
37.63	3.560		.771	.771		.771	.770		.773	.767		.779	.756		.801	.710		1.571	1.486	
39.38	3.639		1.152	1.152		1.153	1.152		1.155	1.149		1.160	1.138		1.182	1.093		2.334	2.245	
41.13	3.695		1.439	1.439		1.440	1.439		1.440	1.435		1.447	1.425		1.469	1.381		2.908	2.820	
42.88	3.724		1.595	1.595		1.595	1.594		1.597	1.592		1.603	1.581		1.625	1.538		3.220	3.133	
43.75	3.727		1.610	1.610		1.610	1.609		1.612	1.607		1.618	1.596		1.640	1.553		3.250	3.163	
44.62	3.724		1.595	1.595		1.595	1.594		1.597	1.592		1.603	1.581		1.625	1.538		3.220	3.133	
46.37	3.695		1.439	1.439		1.440	1.439		1.440	1.435		1.447	1.425		1.469	1.381		2.908	2.820	
48.12	3.639		1.152	1.152		1.153	1.152		1.155	1.149		1.160	1.138		1.182	1.093		2.334	2.245	
49.87	3.560		.771	.771		.771	.770		.773	.767		.779	.756		.801	.710		1.571	1.486	
50.75	3.515		.563	.563		.562	.561		.564	.558		.570	.547		.592	.500		1.154	1.062	
51.62	3.468		.358	.358		.358	.357		.360	.354		.366	.343		.390	.296		.748	.654	
52.50	3.420		.170	.170		.171	.170		.173	.167		.178	.155		.202	.107		.373	.278	
53.37	3.376		.026	.026		.027	.026		.029	.023		.035	.011	1.202	.054	0	1.500	.084	0	
53.56	3.369		.012	.012		.012	.011		.014	.008	.750	.021	0	.920	.032	0	1.150	.049	0	
53.75	3.361	0	0	0	0	0	0	0	0	0	0	0	0	0	0	0	0	0	0	
79.62	1.514	Radii the same for all bodies																		

Radii for bodies 9 through 14 are the same as for body 8. All dimensions are in inches.

TABLE I.- COORDINATES OF BODIES - Concluded
 (c) Vertical ordinates, z , for modifications 2 and 3 to body 2
 (Also see fig. 6)

		Spanwise station y	0	$1/4 r_0$	$1/2 r_0$	$3/4 r_0$
		Body station x				
↑ Modifi- cation 3 ↓	↑ Modifi- cation 2 ↓	30.63	3.275	3.150	2.752	↑ Same as original body 2 ↓
		32.38	3.268	3.206	2.823	
		33.75	3.034	3.169	2.870	
		33.94	2.981	3.149	2.881	
		34.13	2.918	3.126	2.914	
		35.00	2.552	2.927	2.993	
		35.88	2.187	2.548	3.056	
		36.75	1.886	2.185	3.039	
		37.63	1.633	1.884	3.881	
		39.38	1.254	1.449	2.193	
	41.13	1.017	1.190	1.702		
	42.88	.902	1.066	1.644		
	43.75	.888	1.053	1.623		
	44.62	.902	1.066	1.644		
	46.37	1.017	1.190	1.702		
	48.12	1.254	1.449	2.193		
	49.87	1.633	1.884	3.881		
	50.75	1.886	2.185	3.039		
	51.62	2.187	2.548	3.056		
	52.50	2.552	2.927	2.993		
	53.37	2.918	3.126	2.914		
	53.56	2.981	3.149	2.881		
	53.75	3.034	3.169	2.870		
	55.12	3.268	3.206	2.823		
	56.87	3.275	3.150	2.752		

All dimensions are in inches

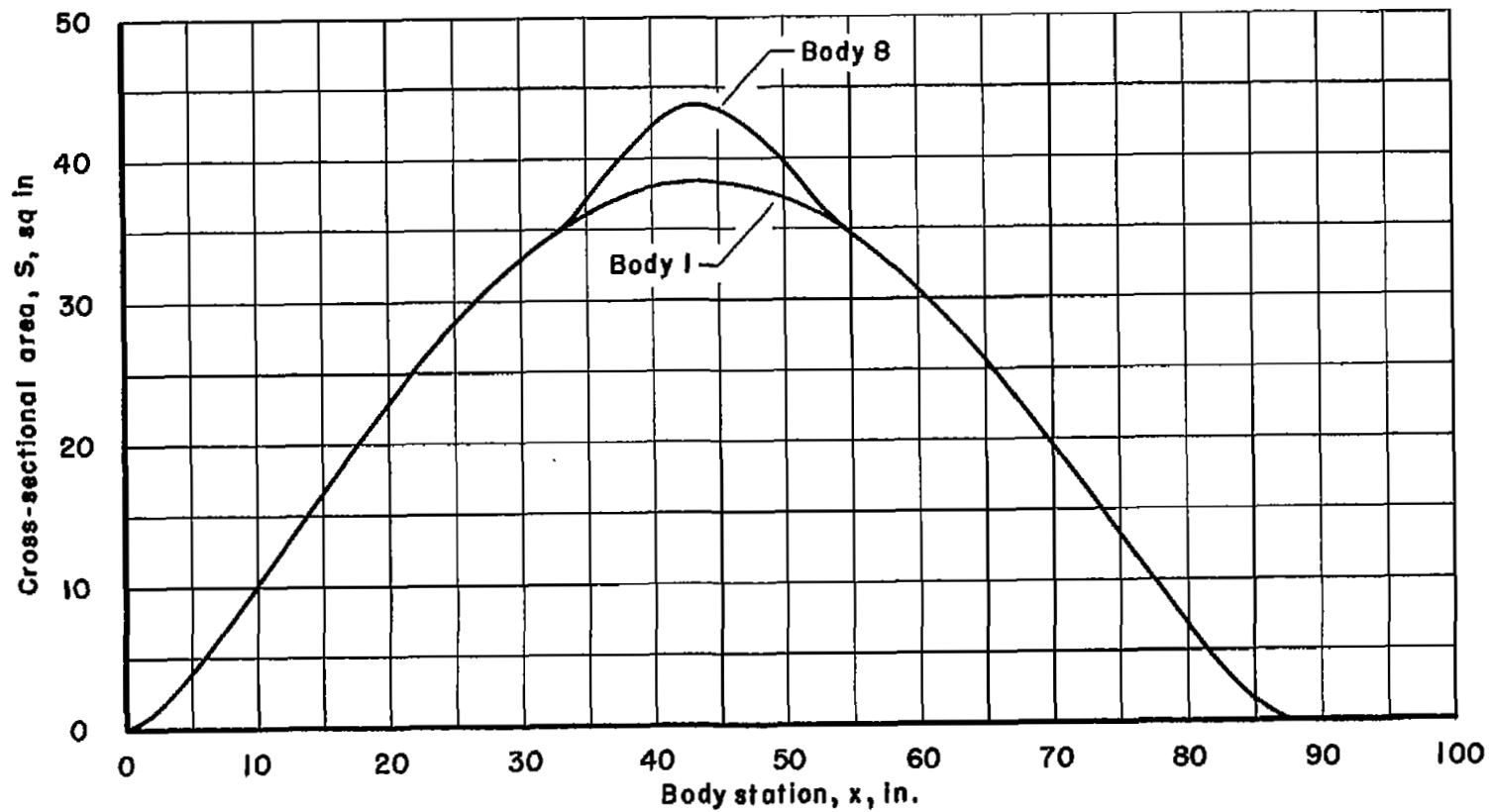
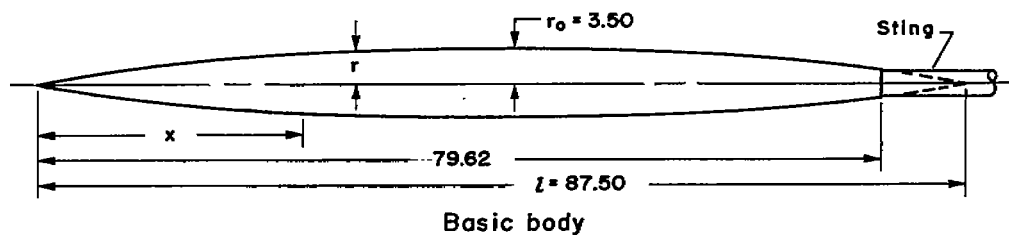
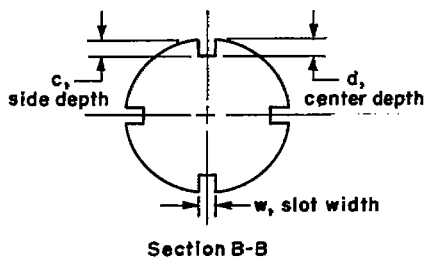
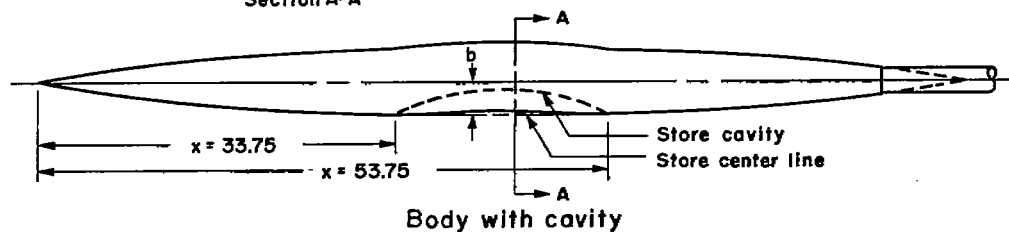
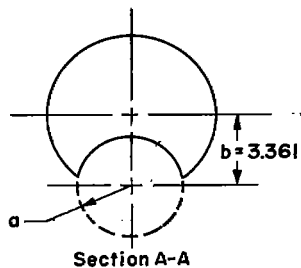


Figure 1.- Area distributions for the basic Sears-Haack body (body 1) and body 8.

Equation of fuselage radii, $\frac{r}{r_0} = \left[1 - \left(1 - \frac{2x}{l} \right)^2 \right]^{3/4}$



Dimensions in inches



See table I for coordinates of bodies with cavities and slots

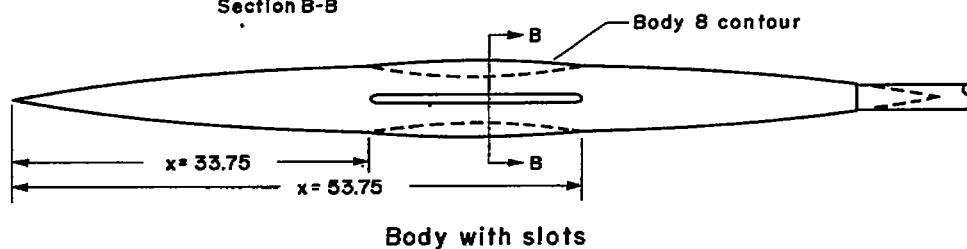


Figure 2.- Sketches of the basic Sears-Haack body (body 1), a body with a cavity (body 2), and a body with slots (body 12).

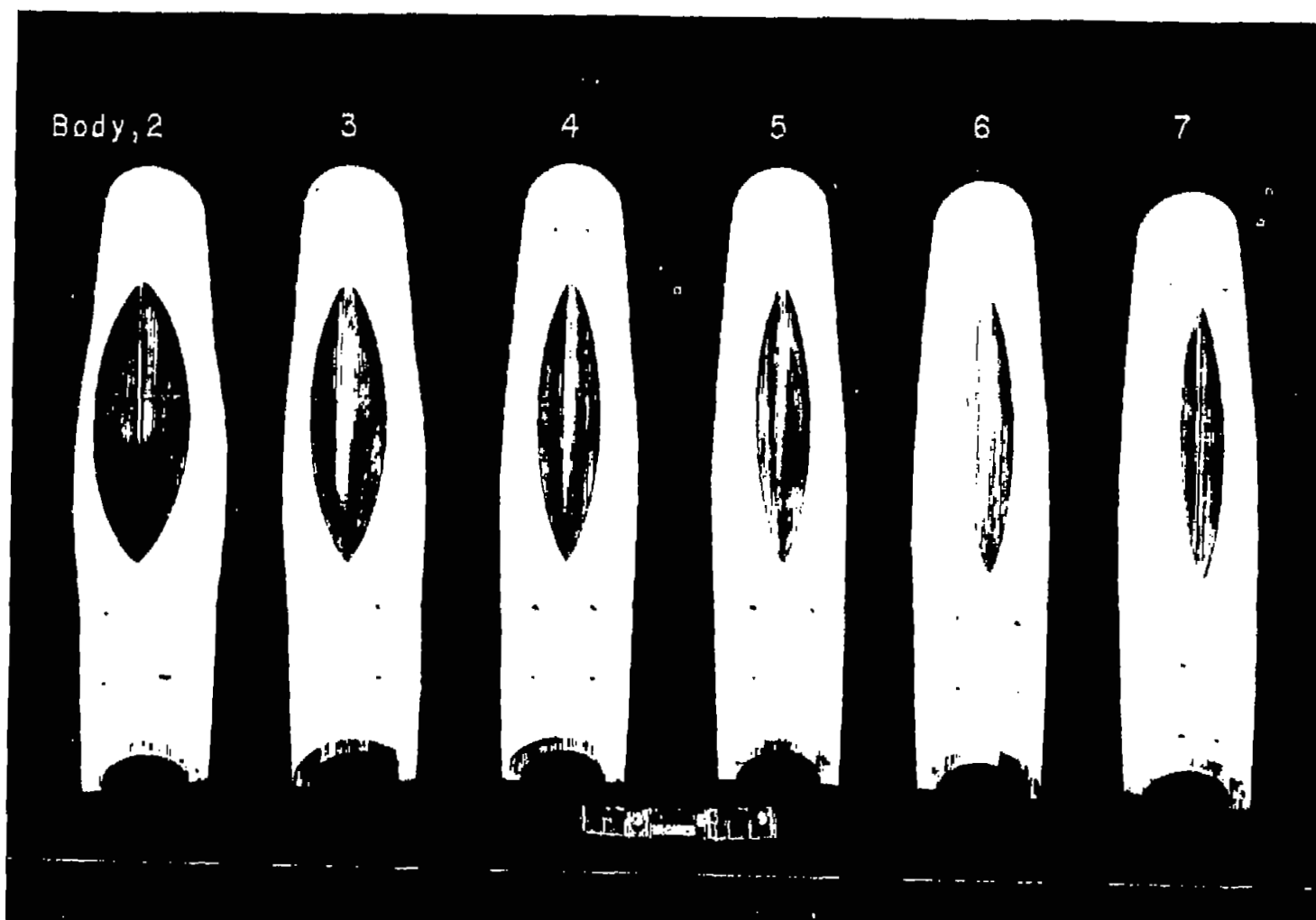


Figure 3.- Lower halves of the central segments of bodies 2 through 7, with cavities.

A-22488.1

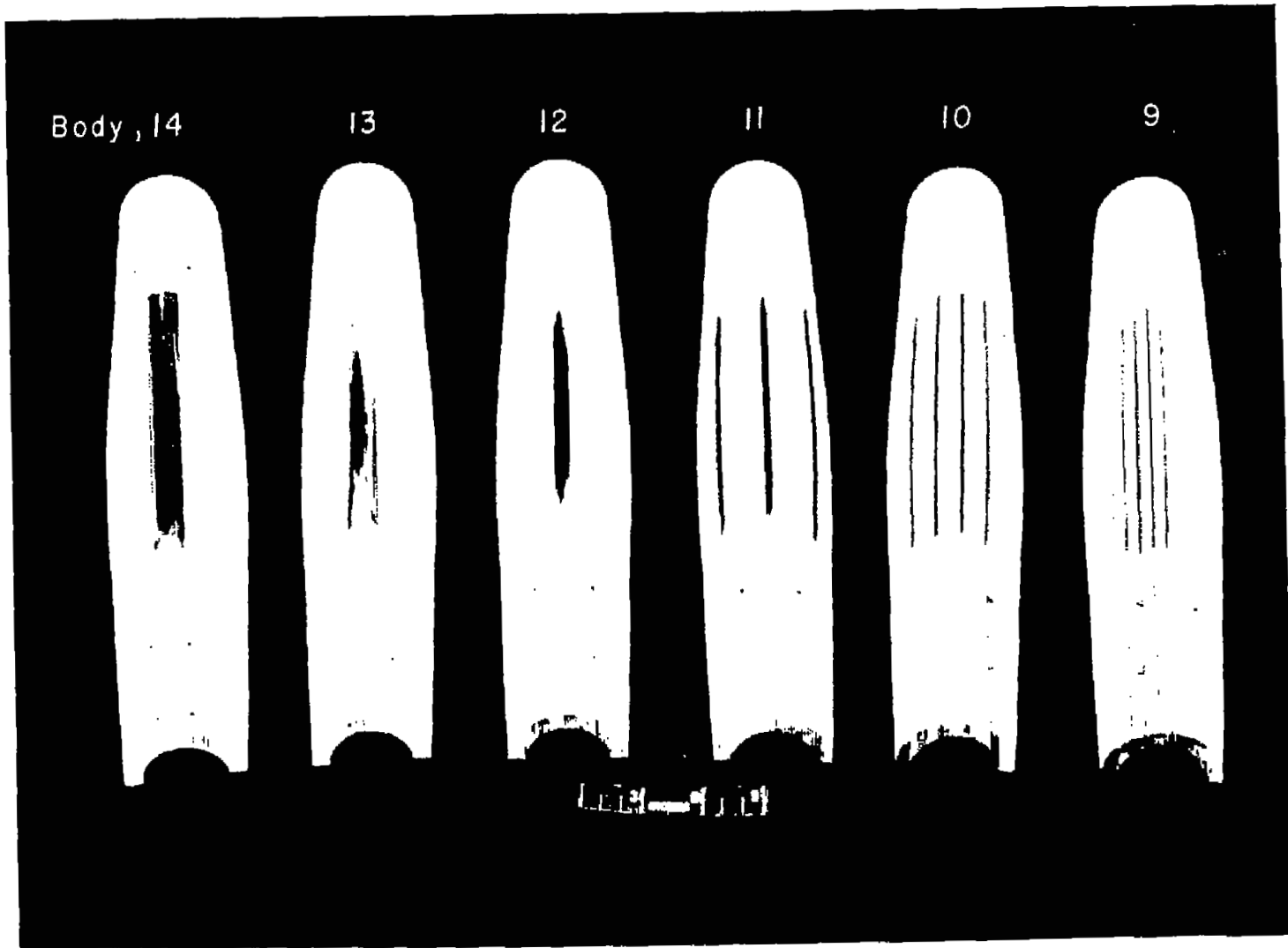


Figure 4.- Lower halves of the central segments of bodies 9 through 14, with slots.

A-22455.1

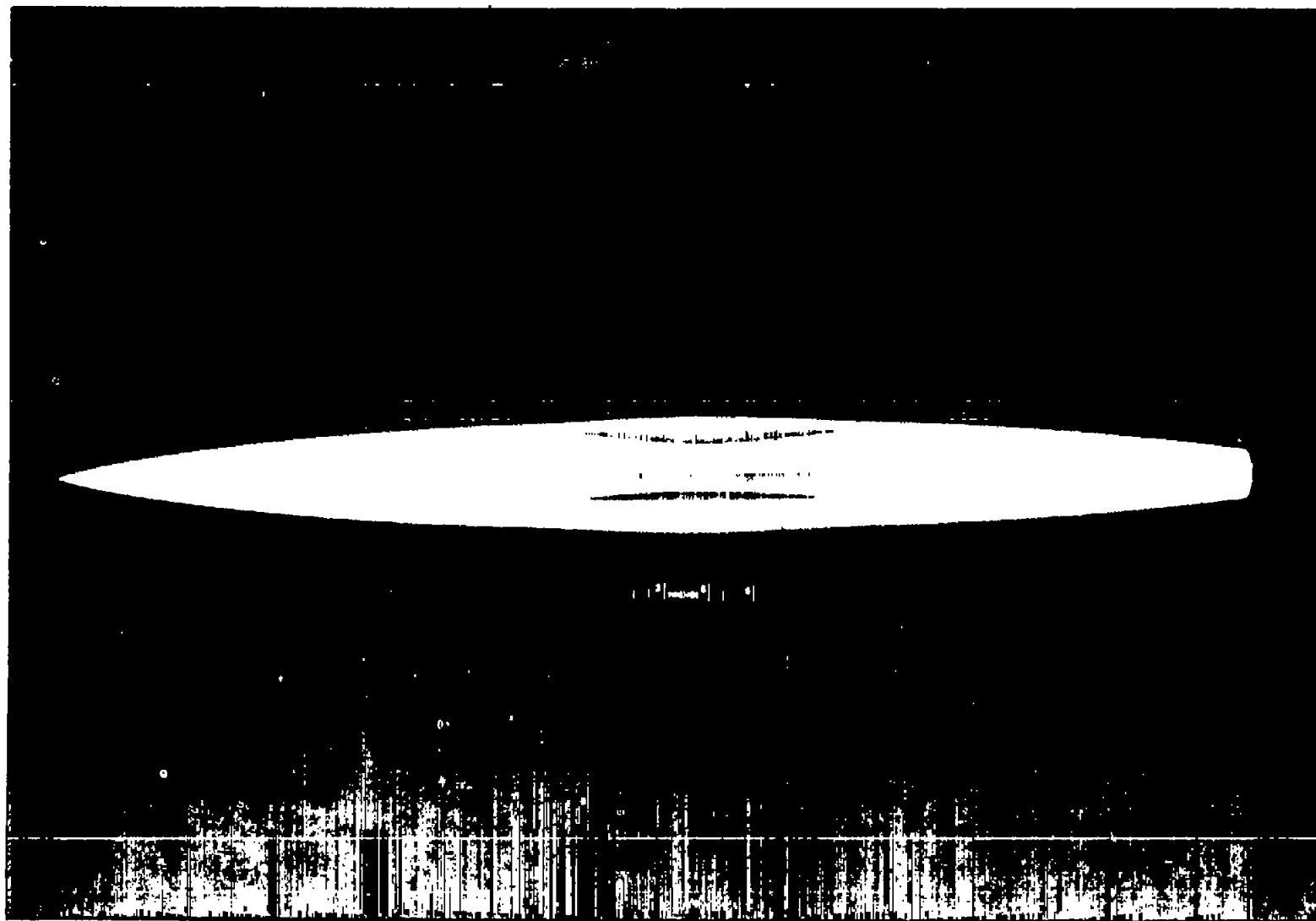


Figure 5. - Modified body 13 with two slots in an asymmetric location.

A-22534.1

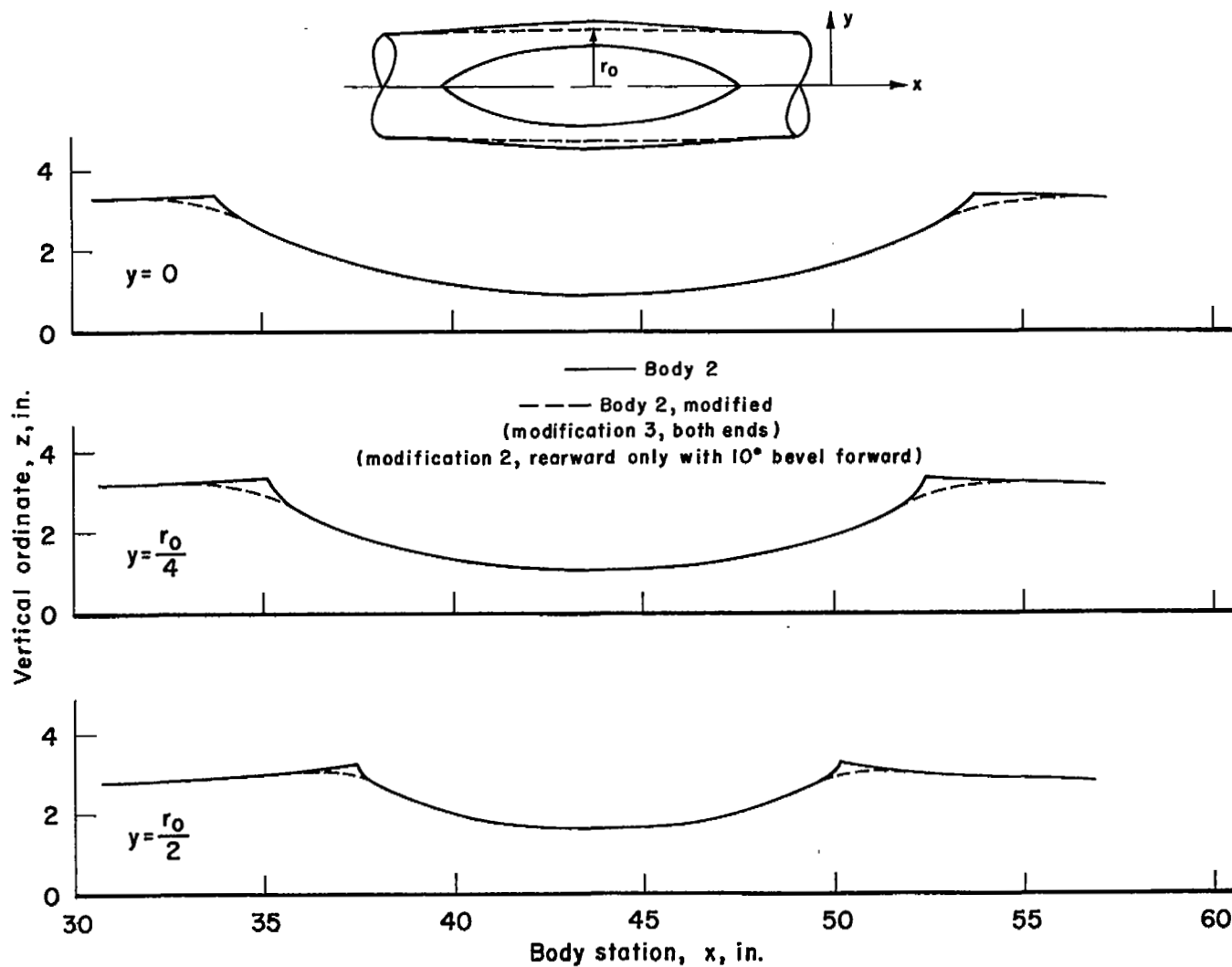


Figure 6.- View of section cuts parallel to the xz plane of body 2 with and without beveled edges.

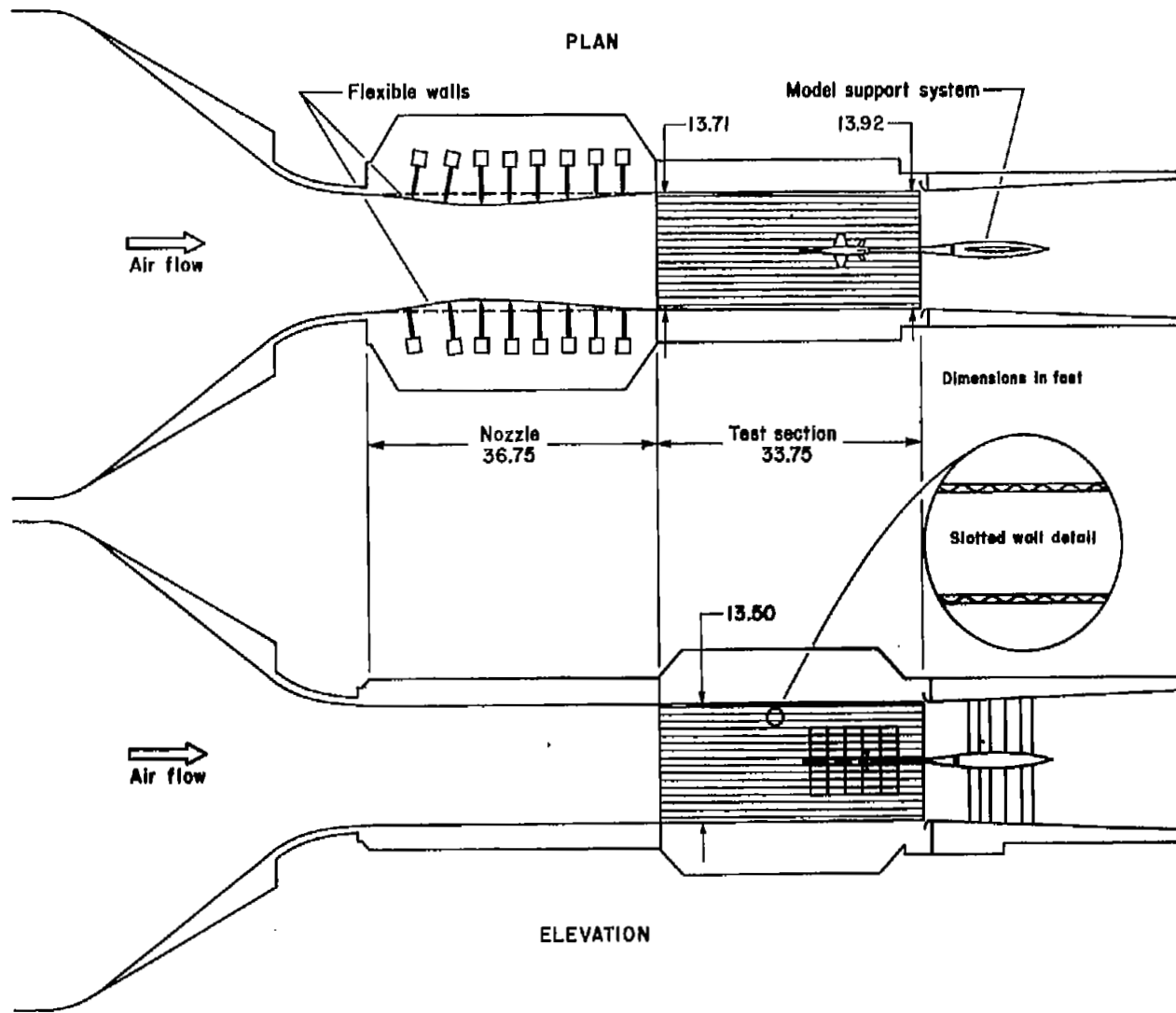


Figure 7.- Two views of the high-speed region of the Ames 14-foot transonic wind tunnel.



A-22458.1

Figure 8.- Basic Sears-Haack body (body 1) mounted on the sting in the wind tunnel.

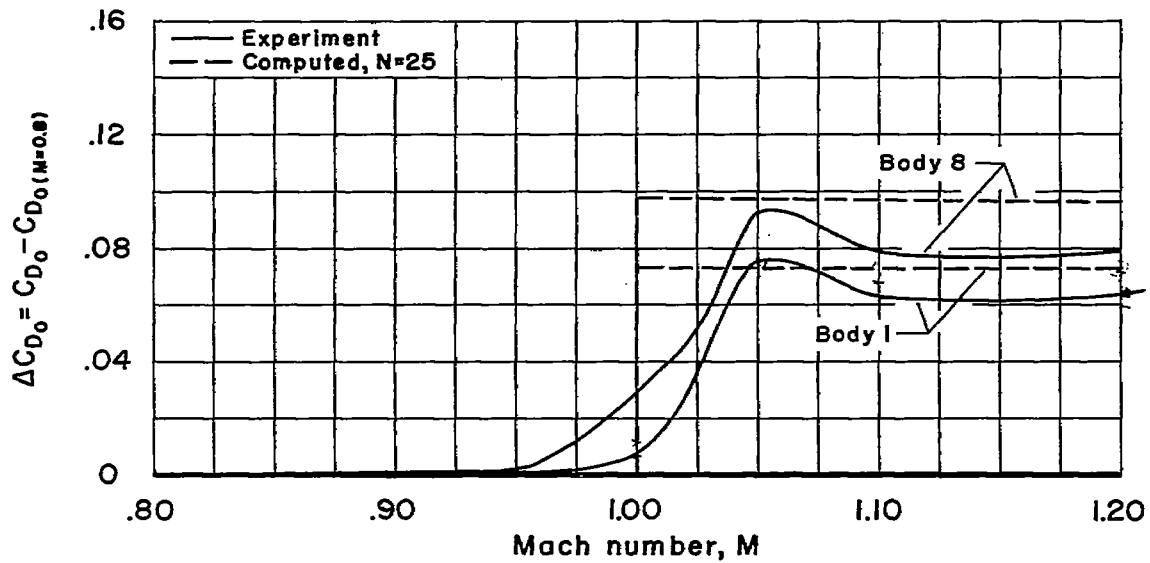
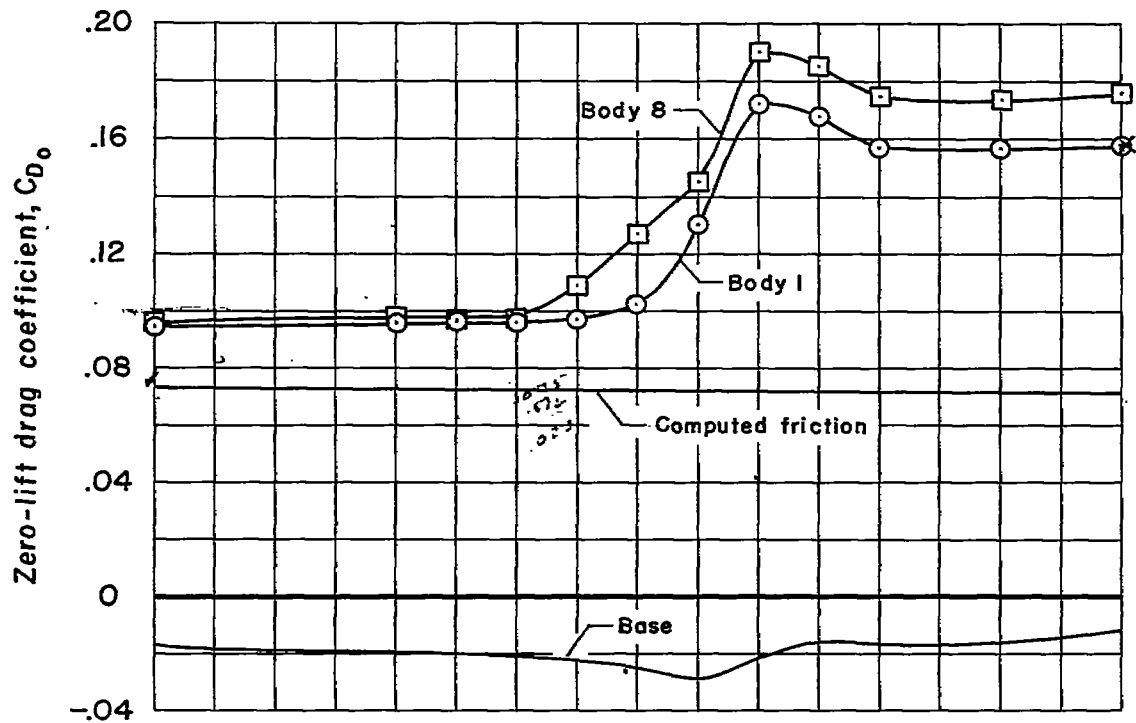


Figure 9.- Drag coefficients for the basic Sears-Haack body (body 1) and body 8.

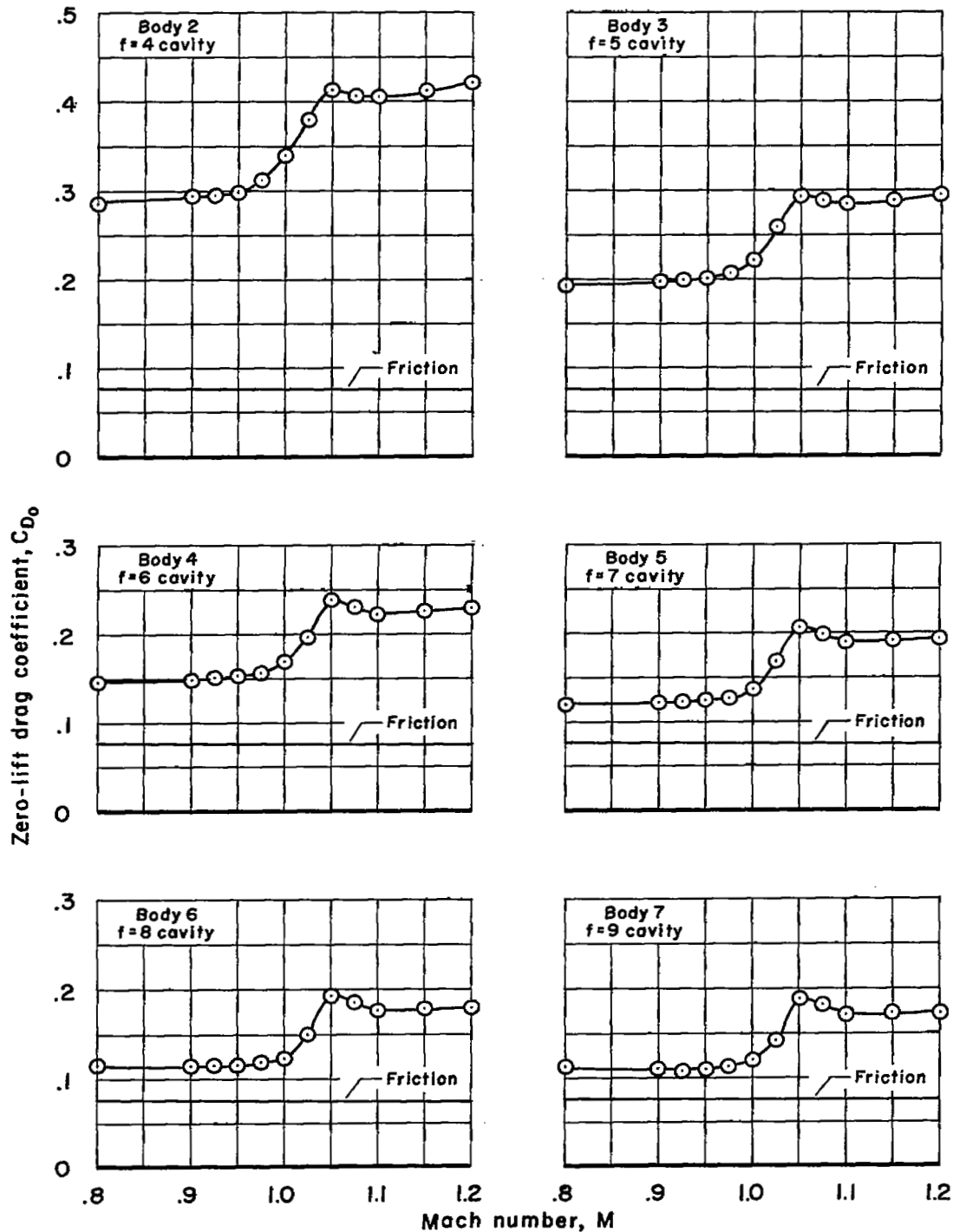


Figure 10.- Experimental drag coefficients and computed friction-drag coefficients for the bodies with cavities.

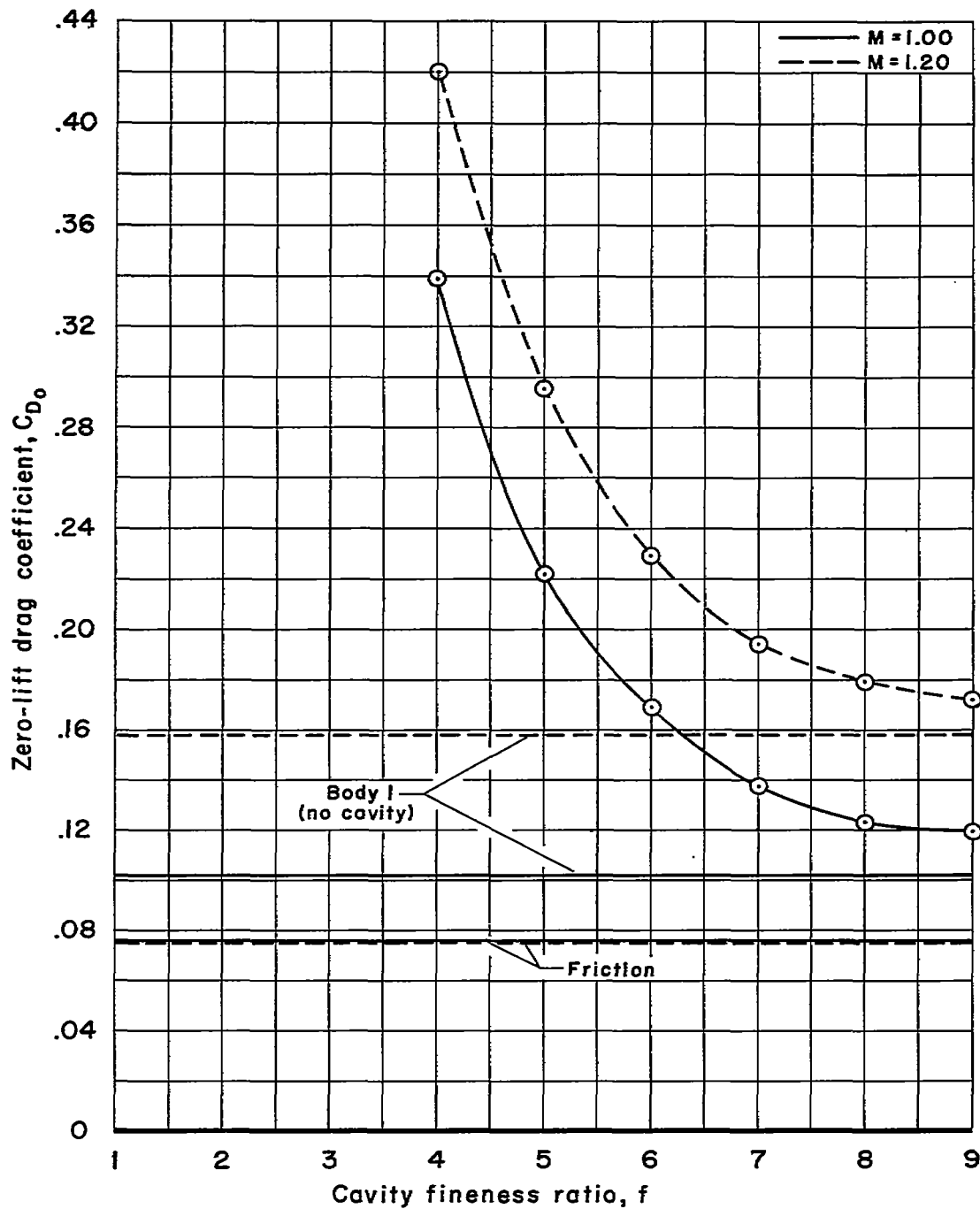


Figure 11.- Variation with cavity fineness ratio of experimental drag coefficients and computed friction-drag coefficients for Mach numbers 1.00 and 1.20.

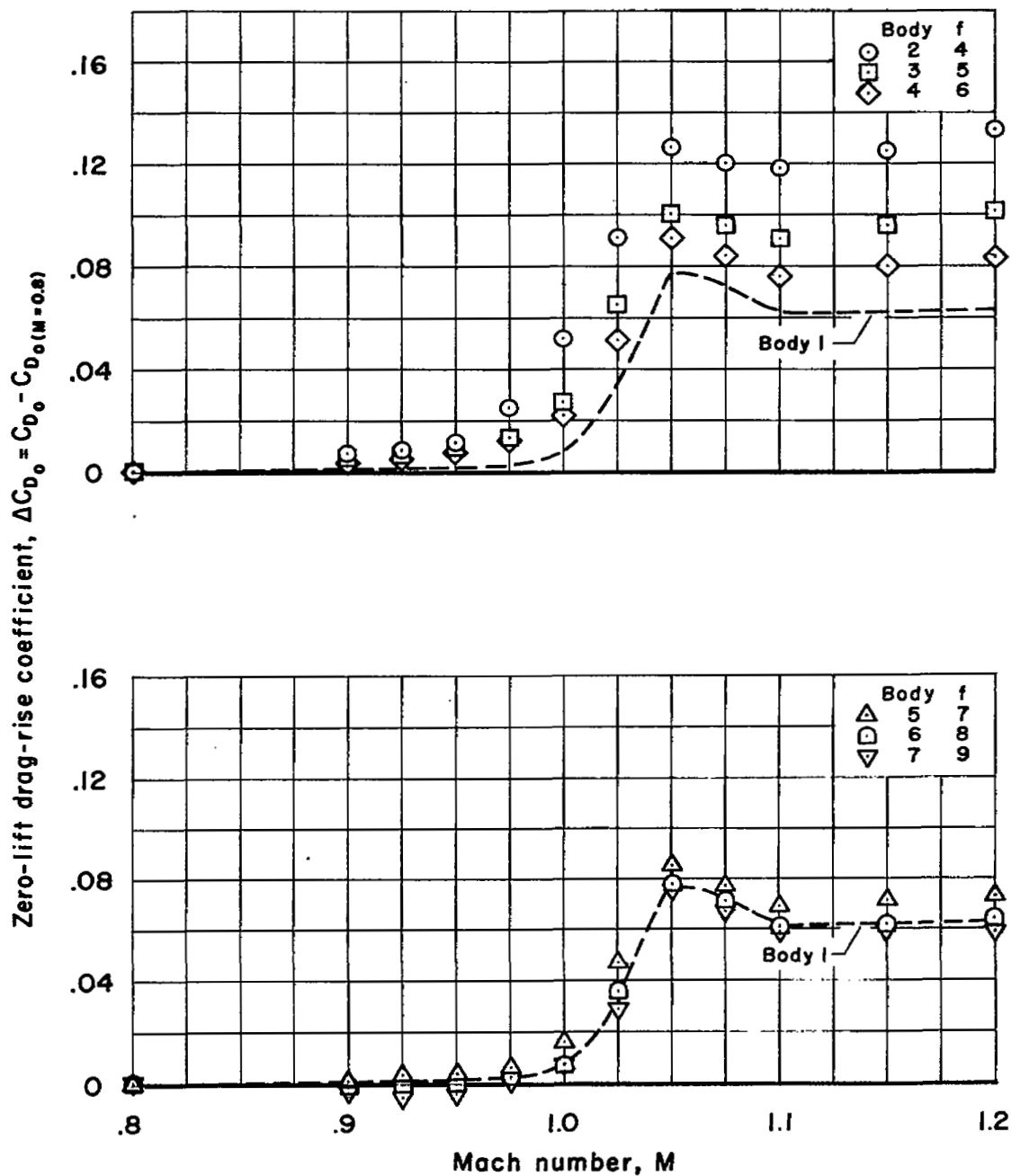
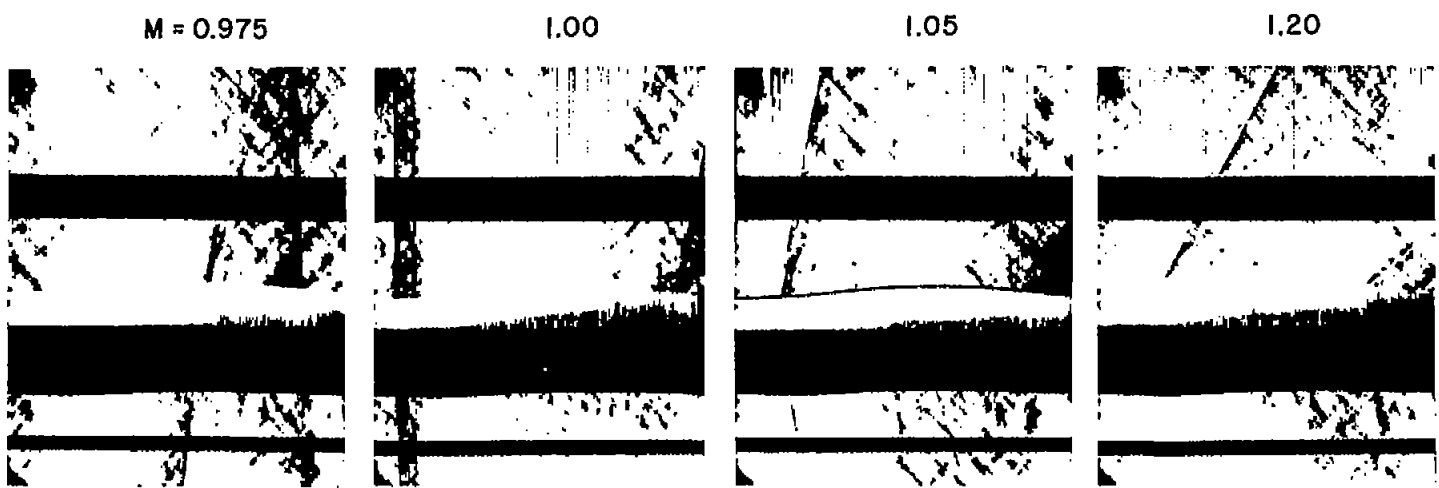
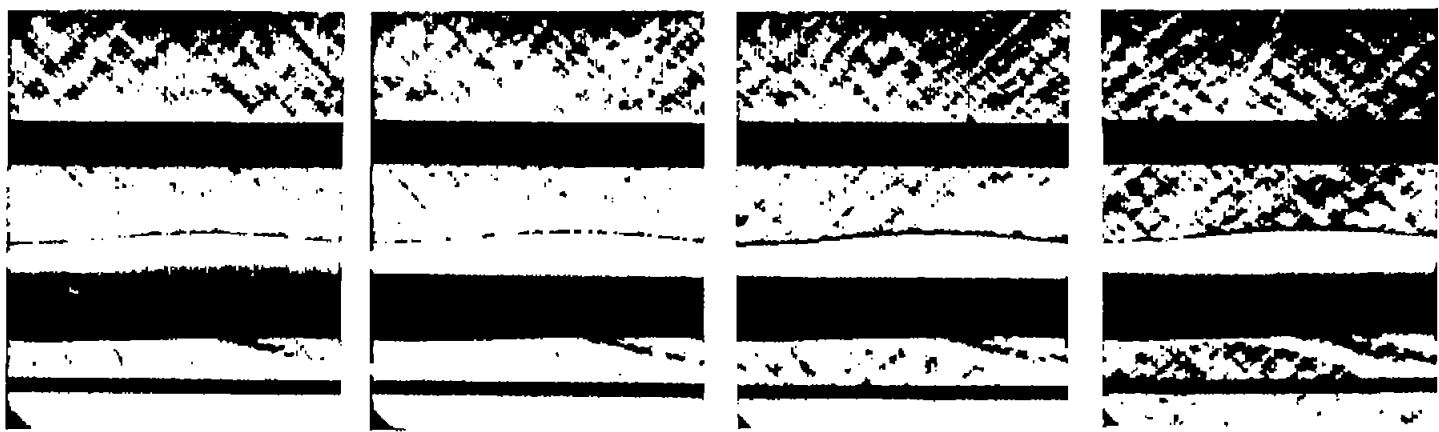


Figure 12.- Experimental drag-rise coefficients above the subsonic level for the bodies with cavities.

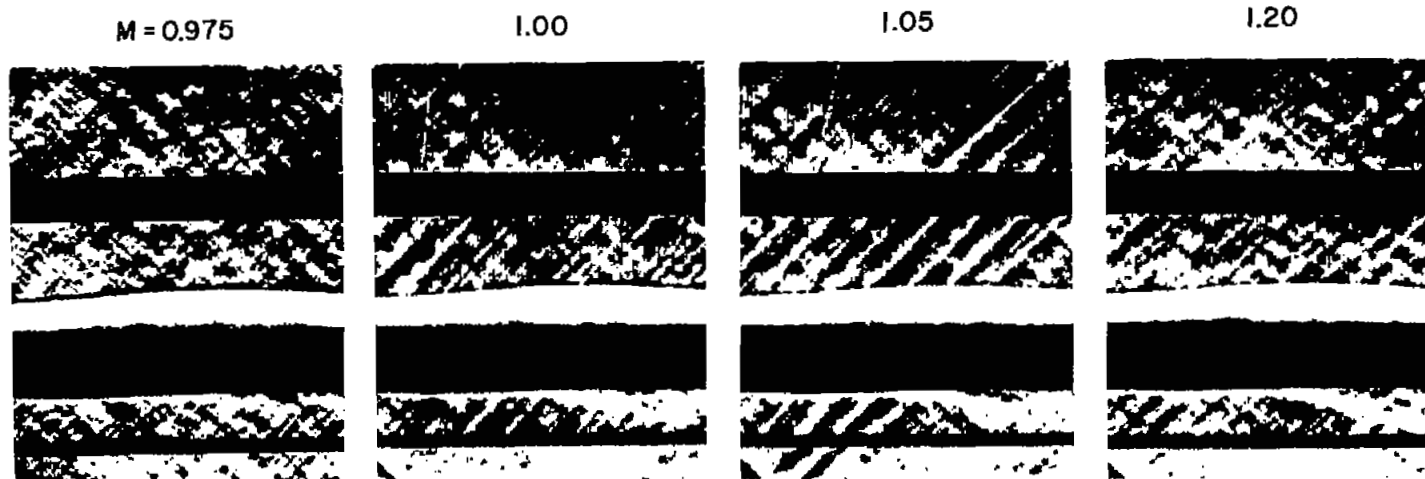


(a) Body 2, $f = 4$ cavity; knife edge vertical.

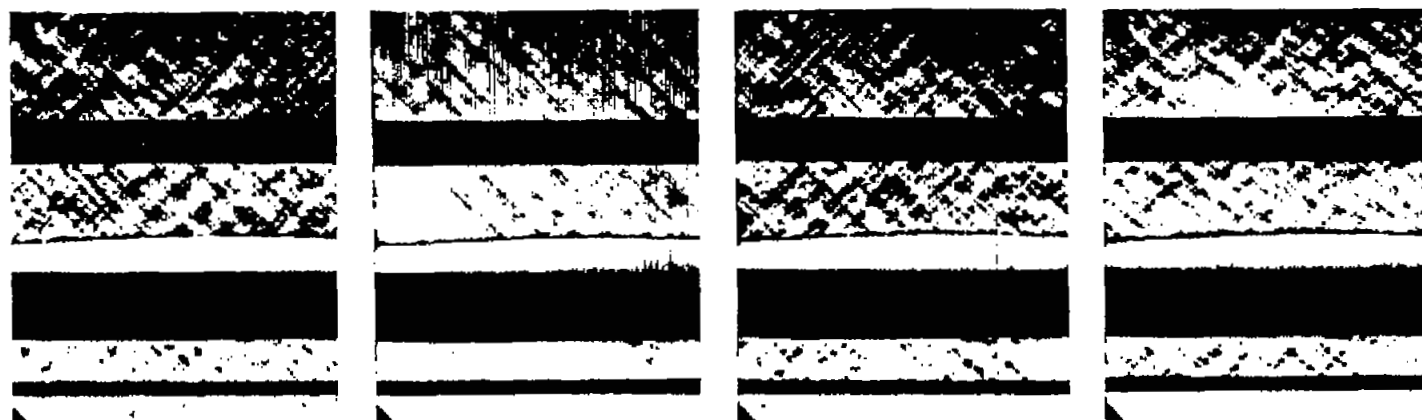


(b) Body 2, modification 2; knife edge horizontal.

Figure 13.- Schlieren photographs of body 2 with the knife edge vertical to accentuate the shock waves and with the knife edge horizontal to accentuate the boundary-layer wake.



(a) Body 3, $f = 5$ cavity; knife edge horizontal.



(b) Body 6, $f = 8$ cavity; knife edge horizontal.

Figure 14. - Representative schlieren photographs showing the decrease in the boundary-layer wake by increasing the cavity fineness ratio.

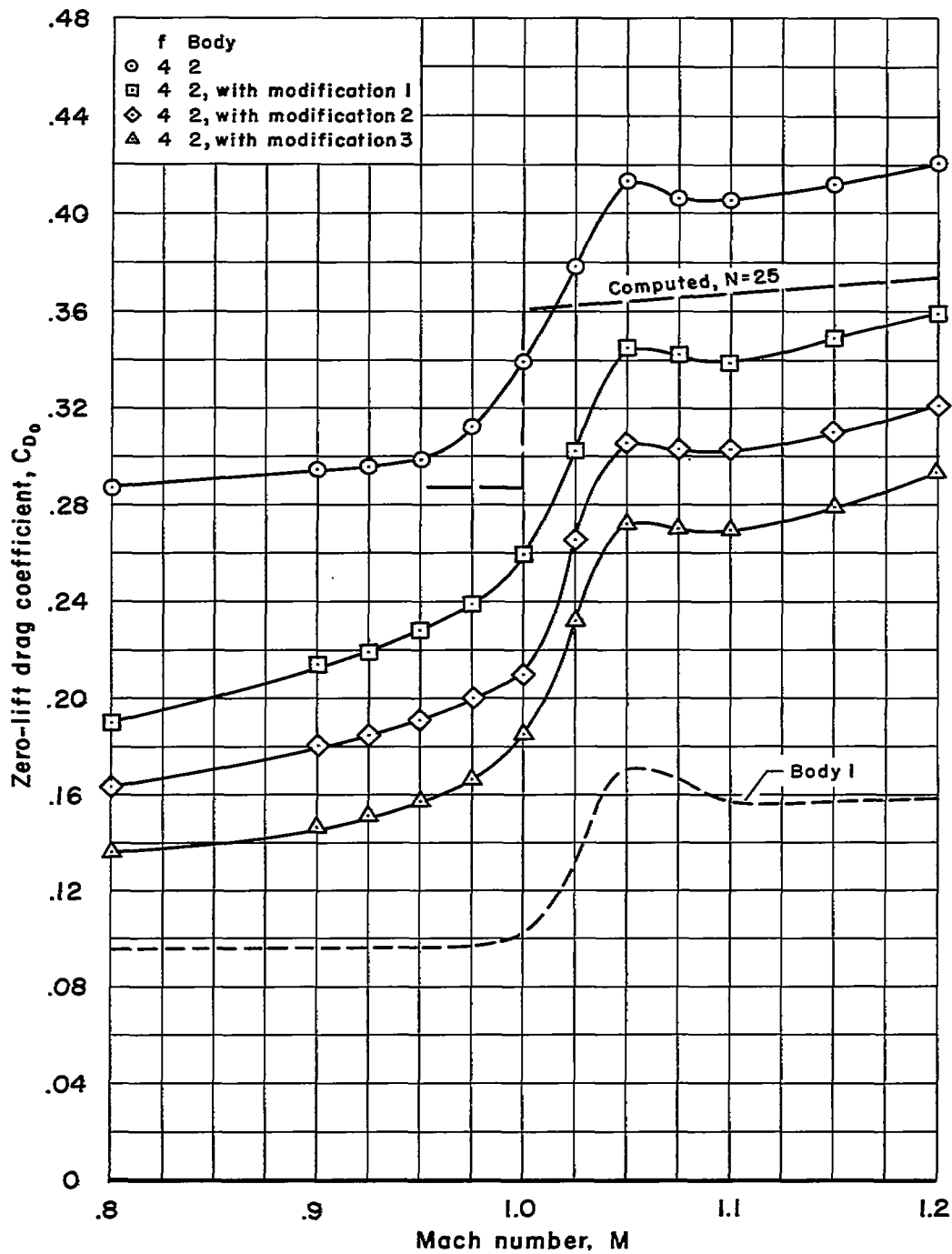


Figure 15.- Experimental drag coefficients for body 2 (f = 4 cavity) and body 2 with modifications.

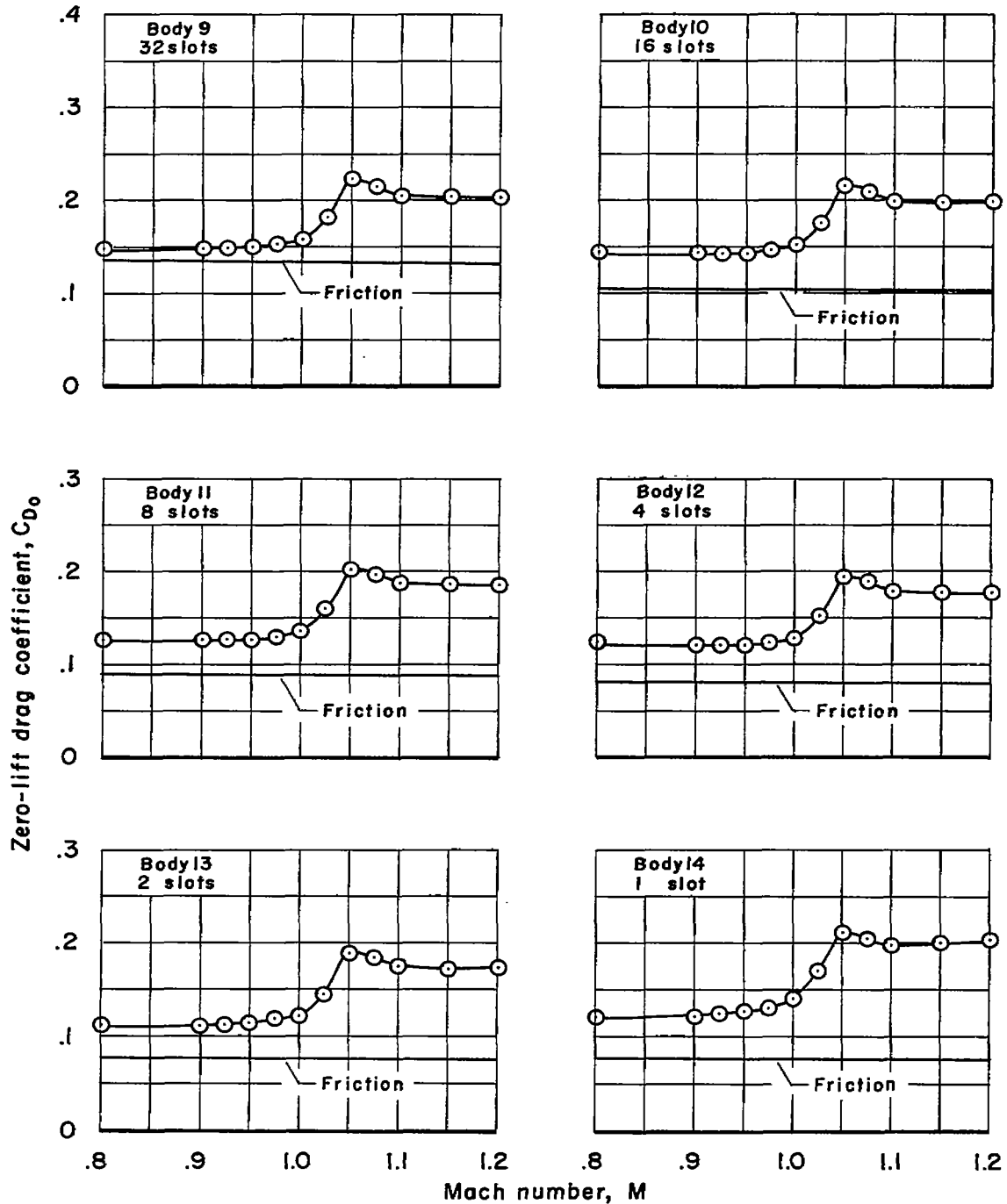


Figure 16.- Experimental drag coefficient and computed friction-drag coefficients for the bodies with slots.

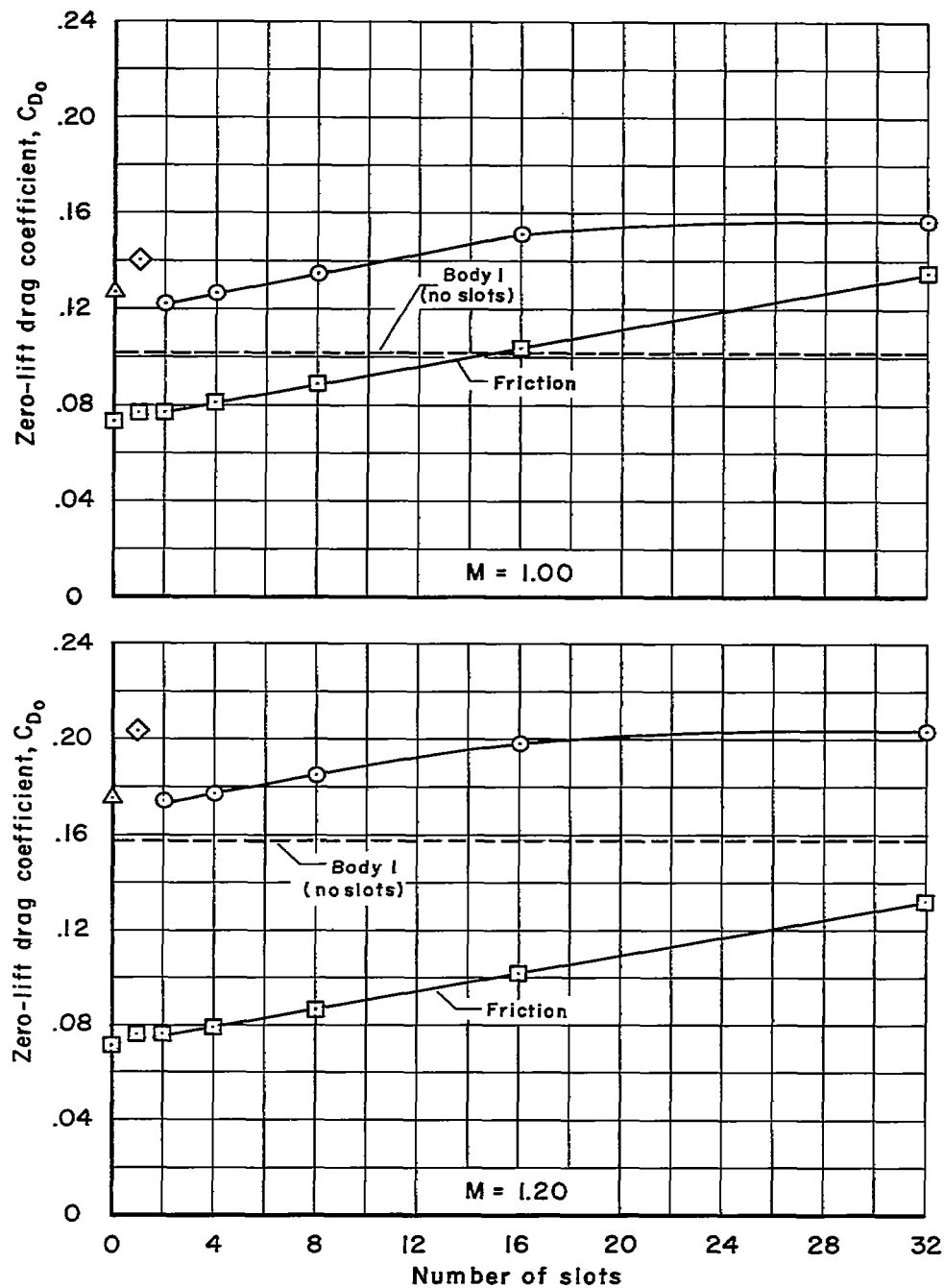


Figure 17.- Variation with number of slots of the experimental drag coefficients and computed friction-drag coefficients for Mach numbers 1.00 and 1.20.

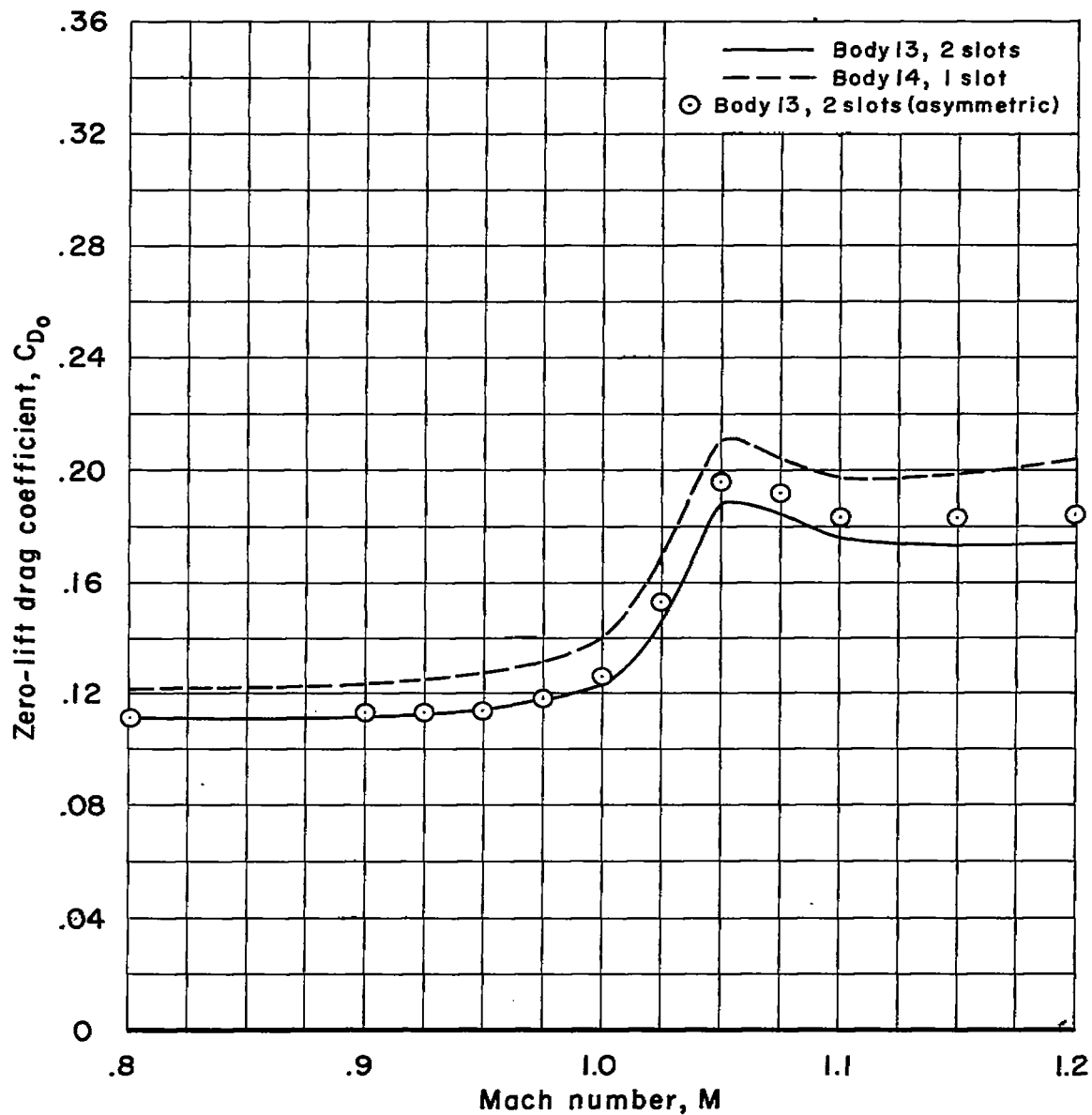


Figure 18.- Drag coefficients for symmetrical and asymmetrical slot locations.

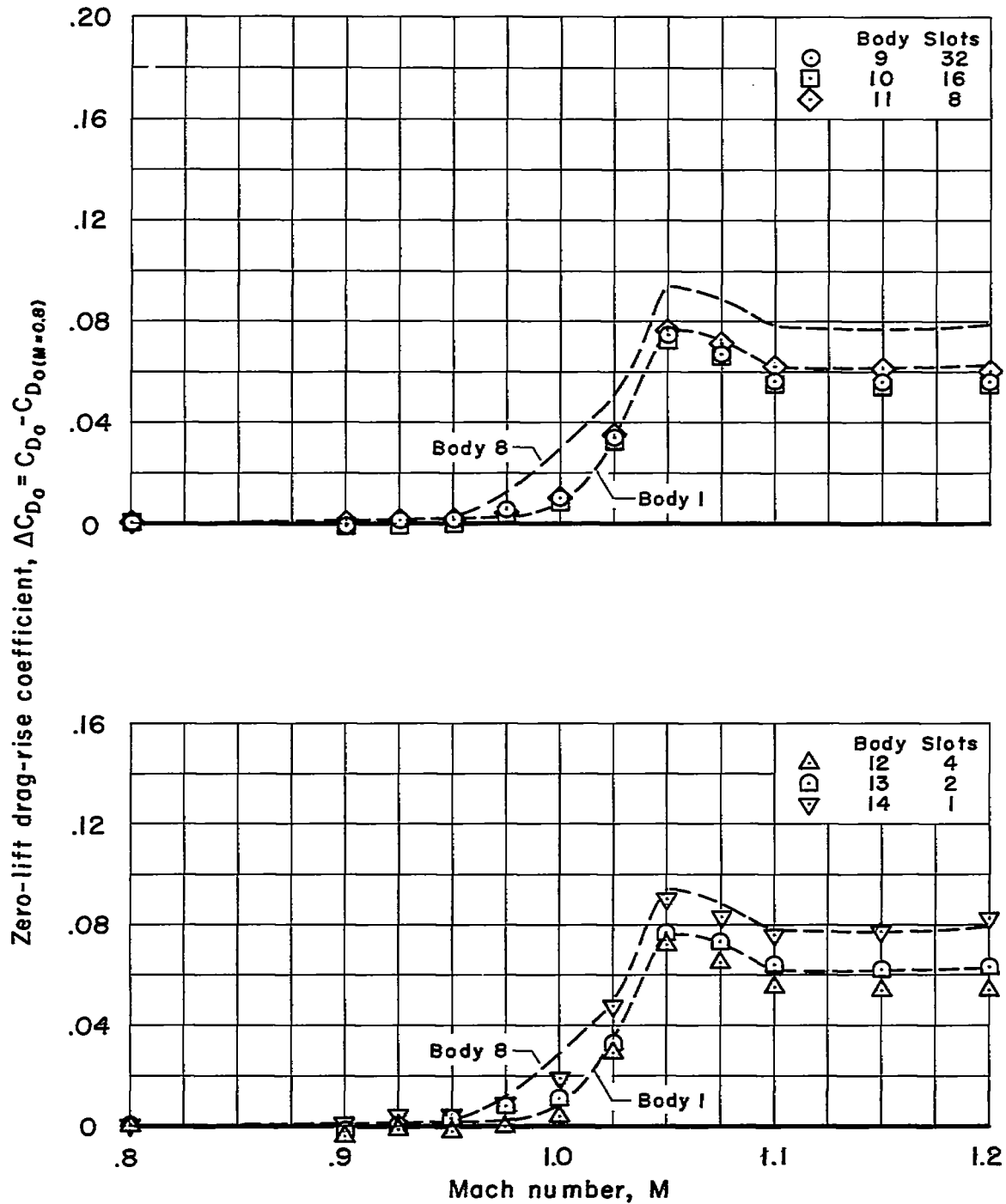


Figure 19.- Experimental drag-rise coefficients above the subsonic level for bodies with slots.



3 1176 01434 9436



1
1

1
1

1
1

